IEEE Access
Multidisciplinary | Rapid Review | Open Access Journal

Received November 19, 2019, accepted November 30, 2019, date of publication December 4, 2019,
date of current version December 18, 2019.

Digital Object Identifier 10.1109/ACCESS.2019.2957534

Study on the Formation and Disassociation Process of Hydrate in Porous Media by Permittivity Dispersion Measurement

BIN WANG, ZHONGHAO ZHANG, AND LANCHANG XING, (Member, IEEE)
College of Control Science and Engineering, China University of Petroleum (East China), Qingdao 266580, China

Corresponding author: Bin Wang (wangbin2015@upc.edu.cn)

This work was supported in part by the National Natural Science Foundation of China under Grant 51306212 and Grant 41704124, in part by the Fundamental Research Funds for the Central Universities under Grant 16CX05021A, Grant 18CX02112A, and Grant 18CX02176A, in part by the Shandong Provincial Natural Science Foundation under Grant ZR2019MEE095 and Grant ZR2017BEE026, and in part by the Shandong Province Key Research and Development Plan, under Grant 2018GGX101020.

ABSTRACT To develop a more efficient and environmentally friendly exploitation and production method of gas hydrate, a better understanding of the formation and disassociation process mechanism of gas hydrate in porous media is indispensable. The permittivity spectra of gas hydrate differs from water, oil, ice and gas, and thus measurement of its permittivity properties is a potential approach to detect hydrate existence and content. In this study, THF (tetrahydrofuran) was used as the hydrate former. The permittivity dispersion of hydrate in quartz sand was measured with open-ended coaxial method in the processes of formation and disassociation at a wide radio frequency band from 1MHz to 3GHz. From the dielectric measurements, the hydrate concentration in the porous media was identified with dispersion properties, and the characteristic of the permittivity response upon the hydrate formation and dissociation were also provided. Moreover, by applying dielectric mixing models, the fractions of the solution and hydrate could be estimated. These results implied that the permittivity dispersion could be an effective monitor for the formation and disassociation of the hydrate, and hydrate content could be evaluated in real time with complex permittivity spectra.

INDEX TERMS Complex permittivity, dielectric measurement, dielectric dispersion, gas hydrate, open-end coaxial line, porous media.

I. INTRODUCTION

Clathrate hydrates are crystalline solid compounds consisting of hydrogen-bounded water molecules forming a lattice of polyhedral cages that trap gas molecules [1], [2]. Methane hydrate is abundant in many locations such as sediments and permafrost regions [3]. It was reported that the disassociation of the gas hydrate in reservoir exploitation was caused by depressurization as well as a temperature increase, and hence the dissociation procedure of many kinds of hydrate crystals has been studied and modeled based on data with various experimental methods [4]–[10]. Mechanisms of the formation and dissociation of hydrate crystals in porous media are important to establish efficient techniques for natural gas hydrate exploitation from the sea bottom sediment and tundra in order to avoid geohazards [1], [11], [12]. On the other hand, to develop reliable technology for preventing internal hydrate-plug formation in stored and transported natural gas, it is meaningful to study the formation process of hydrate crystals [13], [14]. For the formation of gas hydrates in emulsions gives rise to a change in the bulk permittivity, the dielectric spectroscopy obtained with open-end probe was found to be a potential technique for the detection of gas hydrates in emulsified systems [15], [16], e.g. to determine the thickness of the hydrate layer (THF and methane-ethane mixture as the hydrate former) deposited on pipeline walls [17] and to monitor hydrate formation in oil-dominated systems [18]. The influence of pressure on the mechanical and electromagnetic properties of gas hydrate was studied, and it was found that the permittivity is a good indicator of the hydrate phase transition [5], [19]–[24]. The dielectric logging tool working at 1.1GHz was used in a hydrate reservoir of Alaska, and the dielectric logs provided similar trends as other logging method such as sonic and induction, with much finer vertical resolution. Practical logging results demonstrated the usefulness of dielectric logging tools for accurately quantifying in-situ gas hydrate saturation [25], [26]. Permittivity spectra provide valuable information not obtainable from

The associate editor coordinating the review of this manuscript and approving it for publication was Abhishek K. Jha.

single-frequency measurements, however, to the best of our knowledge, there is still little study of the permittivity dispersion of the hydrate contained in porous media reported in the literature.

Open-ended coaxial probes have been used to study permittivity dispersion properties of hydrate deposits in Water/Oil emulsions and metal pipe [18]. By measuring a broad frequency range, the hydrate agglomeration and deposition can be detected by permittivity spectra [27]. While THF is a Structure II, not Structure I (like methane), hydrate-former, it offers important advantages for laboratory studies, e.g. stability under more obtainable pressure and temperature, and complete miscibility in water that guarantees good control on the amount of hydrate formed in sediment samples. For THF hydrate obtains analogical electrical and acoustic properties to methane hydrate, THF has been used as the hydrate former to research hydrate's physical properties and interaction with the porous media in many published studies [5]–[7], [28]. In addition, laboratory dielectric spectroscopy measurements of liquids, semisolids and biological materials (e.g. muscles and tubers) in a wide microwave frequency range are presented in recent years, and new measurement methods for determination of complex permittivity have been developed [29]–[33]. Complex permittivity as function of many factors e.g. water content, temperature, salinity and pressure are tending to be studied in broader frequency ranges [34], [35]. The open-ended coaxial probe is very attractive due to its applicability to nondestructive measurements of complex permittivity in a wide microwave frequency range, which can cover the dispersive frequencies of both hydrate and liquid solution simultaneously(1MHz-13.6GHz) [27]. However, concerning the existing studies on dielectric properties of gas hydrate [5]–[7], there was still no research on formation and dissociation process of hydrate in porous media with dielectric spectroscopy.

In this study, permittivity properties of THF hydrate's formation and disassociation processes in both its pure state and quartz sand were studied using open-ended coaxial probes, and an evaluation method based on the permittivity dispersion of the hydrate fraction in porous media was studied. The results demonstrated that dispersion characteristics of complex permittivity spectra on broadband can indicate the existence of the THF hydrate and THF solution together. Furthermore, there are evident differences in the permittivity under 100MHz between the ice and hydrate [36]–[39], which showed that the permittivity dispersion could be used as a potential technique in approaching in-situ hydrate saturation in tundra reservoirs. By applying proper mixing laws, fractions of each component can be precisely evaluated at any period of the experiments.

II. EXPERIMENTAL METHODOLOGY

A. PERMITTIVITY DISPERSION

The permittivity spectrum measuring the dielectric constant and loss factor of materials is always dispersive in the frequency domain, and it is a complex value normally related to other physical properties [40], defined as:

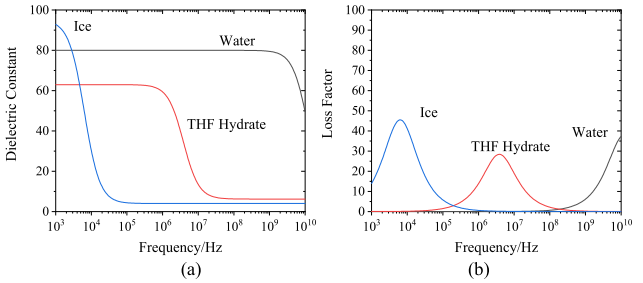

FIGURE 1. Real part (a) and imaginary part (b) of the complex permittivity of ice (blue), the THF hydrate (red), and water (black).

$$\varepsilon^* = \varepsilon' - j\varepsilon'' \tag{1}$$

where ε^* is the complex relative permittivity, and the real part ε' and imaginary part ε'' refer to the dielectric constant and loss factor, respectively. When an alternating electromagnetic field is applied to the material, several polarization phenomena such as the Maxwell-Wagner effect, displacement of the electronic cloud of atoms, and orientation of polar molecules contribute to the dispersion of the permittivity. The dielectric constant can be interpreted as the net polarization of opposing the applied EM field, and the loss factor is related to the transformation of EM energy to joule heat and polarization loss. Typical complex permittivity spectra of the THF hydrate, ice, and liquid water from 1 kHz to 10 GHz are illustrated in Fig. 1 [41], [42].

The permittivity spectroscopy of THF hydrates, ice, and liquid water can be numerically described as a Cole-Cole model [43].

$$\varepsilon(\omega) = \varepsilon' - j\varepsilon'' = \varepsilon_\infty + \frac{\varepsilon_s - \varepsilon_\infty}{1 + (j\omega\tau)^{1-\alpha}} - j\frac{\sigma}{\omega\varepsilon_0} \tag{2}$$

where $\varepsilon(\omega)$ is the dispersive complex permittivity, ε_s and ε_∞ represent the dielectric constant at static and infinity frequency, respectively, ω is the radian frequency, α is an index parameter less than 1, τ is the relaxation time in sec, and σ is the conductivity

As shown schematically in Fig 1, the prominent dispersion of liquid water's permittivity spectrum caused by the molecular polarization can be observed above 1GHz, while ice and clathrate hydrates are characterized by a wide region of the dielectric dispersion and absorption below 10MHz. For clathrate hydrates, the dispersion depends not only on the relaxation of water but also on the nature of the encaged guest molecules, and may considerably vary with guest molecules [37], [42], [44]. Thus, the hydrate has distinct dispersion characters from both the ice and liquid solution, and consequently, the hydrate formation and disassociation can be monitored by the permittivity spectrum measurement.

B. EXPERIMENT DESIGN

This research was conducted using an instrument as sketched in Fig 2. A plugged glass reactor containing porous media and the THF solution was placed in a program

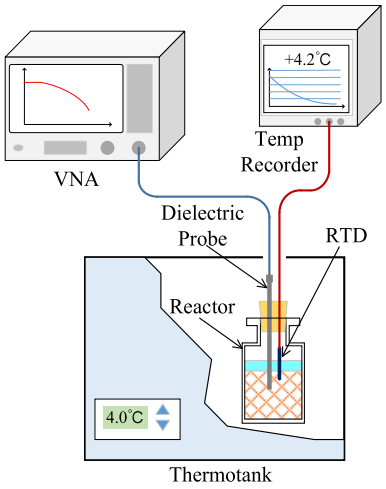

FIGURE 2. Schematics of the experimental equipment. The control accuracy of the thermotank was ±0.5°C and the precision of the temperature recorder with the RTD was is ±0.15°C. The glass reactor was sealed by a plug preventing volatilization of the solution. The slim-type dielectric probe and the conductor wire for the RTD pierced through the plug to penetrate into the media.

controlled thermotank. To form or dissociate the hydrate, the reactor was cooled to −12°C or warmed to room temperature with an automatic program control. A slim-type open-ended coaxial probe (from Keysight, outer conductor's diameter of 2.2mm, inner conductor's diameter of 0.53mm, insulation layer between the two conductor is Teflon) was connected to a VNA (Vector Network Analyzer from Keysight, model: 5061B) with a 50 Ohm phase-stable cable penetrating into the measured media inside the reactor, and the complex permittivity was acquired with N1500A software installed on the VNA. The measurements were obtained after a calibration by measuring three known reflection coefficients (25°C deionized water, air and a short kit were selected as calibration standards). The dispersive permittivity was recorded every minute in a frequency range from 1MHz to 3GHz with the logarithmic coordinate among the whole experimental procession. A Pt100 resistance temperature detector (RTD) mounted in the reactor was used to monitor the temperature of the media and record the temperature variations in real-time.

The THF (>99.9%) and water were mixed at a mass ratio of 1: 4.25 as a hydrate former ($\sigma = 0.05$S/m) that did not remain after the hydrate was formed. Six experiments were carried out, and the porous matrix, initial/ target temperature, and solution fraction are summarized in Table 1. Quartz sand with two particle sizes was prepared as the porous media in experiments 3-6, and the THF solution was supersaturated in order to guarantee that no gas was in the pore spaces. The pure THF hydrate formation and dissociation processes were conducted in experiment 1 and 2 without quartz sand, respectively.

The target temperature of the thermotank was set to −12°C in experiments 1, 3, and 4. The motivation for this was to shorten the formation time and increase the conversion rate of the hydrate. During the cooling period, the temperature of the bathing atmosphere inside the tank was always 3-4°C lower than mixture inside the reactor because of the heat capacity lag. These mixtures were cooled to a supercooling condition, and then hydrate nucleation was triggered by the colder dielectric probe (it acted as a heat conductor through the plug, so the temperature of the probe was between the temperature inside and outside the reactor). Formation started with the temperature suddenly jumping to 4.4°C, and was kept for several hours until the temperature gradually dropped to a lower temperature [22]. The dissociation of the hydrates was triggered by setting the target temperature of the thermotank to room temperature in experiment 2, 5 and 6. Experiment 1 and 4 are terminated before reaching the target temperature because the temperature and permittivity indicated that the formation/ dissociation was completed.

TABLE 1. Configuration details in the experiments.

Experiment Number	Porous matrix and particle size	Initial temperature /°C	Target temperature /°C	Solution fraction
Experiment 1	None	26	-12	100%
Experiment 2	None	-12	20	100%
Experiment 3	Quartz sand 0.45mm-0.9mm	24	-12	60%
Experiment 4	Quartz sand 0.18mm-0.28mm	25	-12	60%
Experiment 5	Quartz sand 0.45mm-0.9mm	-12	18	60%
Experiment 6	Quartz sand 0.18mm-0.28mm	-12	18	60%

III. RESULTS AND DISCUSSION

This section is divided into five parts. First, the dielectric properties of pure THF hydrate will be studied (experiments 1 and 2) in *A*. Then the effect of the porous media on the hydrate formation and dissociation (experiments 3-6) will be investigated in *B* and *C*. The dielectric constant and loss factor at some typical frequency points are illustrated as a function of time, and the effect of the temperature and permittivity on the formation and dissociation processes are concluded. Then, in part *D*, the volumetric fraction is estimated by the dielectric mixing law, and a fitted spectrum is presented and compared with experimental results. Based on the experimental results, the ambiguity and deviations will be analyzed in last part, *E*, and furthermore the peculiarity and advantages of permittivity measurements for the hydrate evaluation in the porous media will be stated.

A. DIELECTRIC PROPERTIES OF THE PURE THF HYDRATE

To better study the THF hydrate deposit in porous media, experiment 1 and 2 were conducted to measure the complex

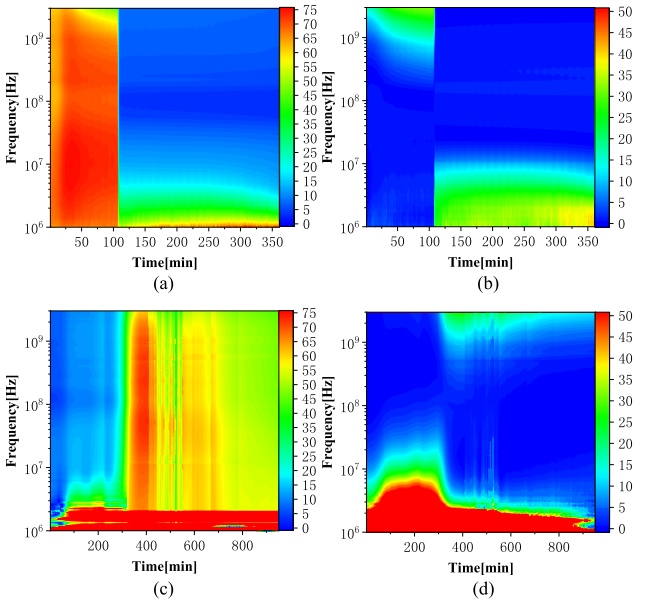

FIGURE 3. Evolution of the complex permittivity spectra as a function of time: (a) effect of the dielectric constant upon the formation process of the pure THF hydrate in experiment 1 (b) effect of the loss factor upon the formation process of the pure THF hydrate in experiment 1 (c) effect of the dielectric constant upon the dissociation process of the pure THF hydrate in experiment 2 (d) effect of the loss factor upon the dissociation process of the pure THF hydrate in experiment 2.

permittivity spectrum during pure THF hydrate formation and dissociation as a control group. Complex permittivity spectra varying with time among the two experiments are illustrated as contour maps in Fig 3.

It can be observed from the contour maps that the characteristic dispersions of the THF solution and THF hydrate were located at a frequency range over 1GHz and below100MHz, respectively. The dispersion of the liquid solution is mainly due to the molecular polarization of water [46]. It makes the dielectric constant large among the whole spectrum, and the loss factor obtains a resonance peak with its center at dozens of GHz (see the range before the 107th min in experiment 1 and after the 250th min in experiment 2). Orientation of restrained water and THF molecules inside the clathrate hydrate contribute to the dispersion peak below 100MHz, so the spectrum's large amplitude below 100MHz could potentially act as the indicator of the hydrate's appearance (see the range after the 107th min in experiment 1 and before the 250th min in experiment 2). Similar spectroscopy properties e.g. dispersion frequencies and their temperature drift of THF hydrate and THF/water solution have been found in the results of formation experiments of pure THF hydrate layers [27].

To evaluate the experimental process more clearly, the complex permittivity at some frequency points (2.5MHz, 3.5MHz, 10MHz, 300MHz, 1GHz and 3GHz are selected as typical frequencies) are presented with recorded temperature in Fig 4. According to the results of experiment 1, both the dielectric constant and loss factor sharply dropped above 20MHz at the 107th min, while a steep

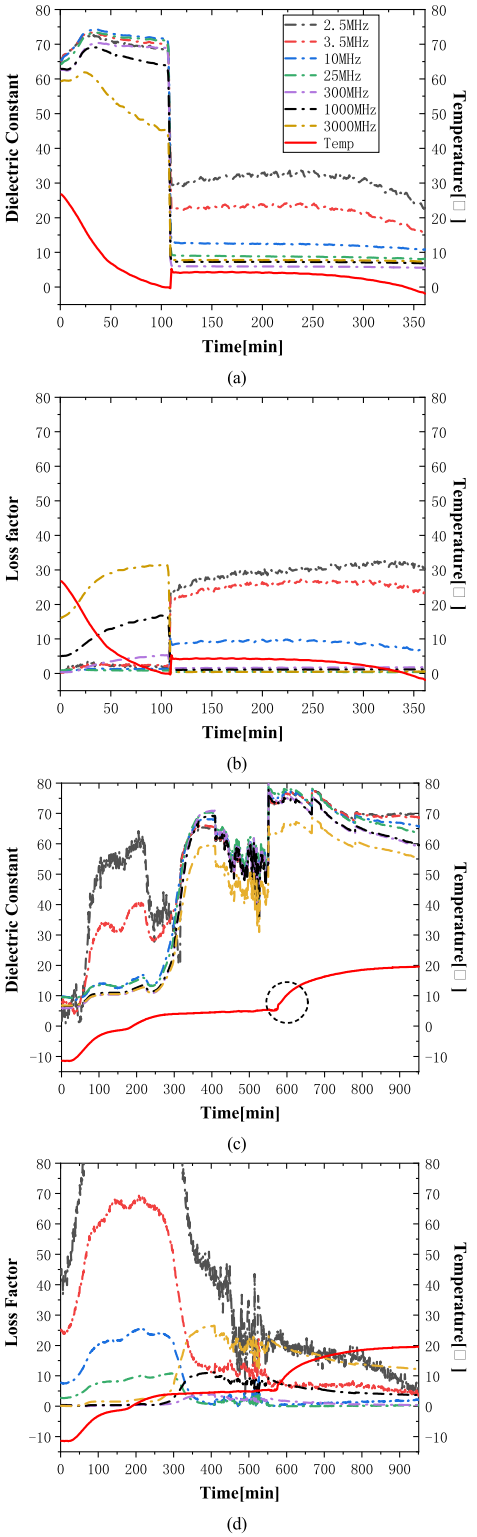

FIGURE 4. Complex permittivity at 2.5MHz, 3.5MHz, 10MHz, 300MHz, 1GHz, and 3GHz and temperature as a function of time. The complex permittivity is plotted with dot dash lines and temperature with solid lines, and the legend that applies to the four subfigures is presented in (a). (a) the effect of the dielectric constant upon the formation process in experiment 1 (b) the effect of the loss factor upon the formation process in experiment 1 (c) the effect of the dielectric constant upon the dissociation process in experiment 2 (d) the effect of the loss factor upon the dissociation process in experiment 2.

temperature rise was observed. For a frequency below 20MHz, peaks appeared with increasing amplitude as the frequency decreased both in the dielectric constant and loss factor. Because the formation of hydrate is exothermic, the temperature jump to 4.4°C vertically at the 107th min indicates that the hydrate has formed in front of the probe's open-end. Compared with the flat and smooth spectrum during the hydrate formation, complex permittivity was observed drastically varying with time during the dissociation process in Fig 3 (c), (d) and Fig 4 (c), (d) before the 550th min.

Considering temperature and complex permittivity synthetically, a stepped change was found at the onset of the formation, while during the dissociation process, the permittivity spectrum fluctuated in a narrow range and the temperature curve was smoother. We drew the conclusion that the dissociation process of the pure THF hydrate is critically slower than its formation, and thus the distribution of the solution and hydrate could be time-varying and more heterogeneous. In addition, as presented in Fig 4(c) and (d), the permittivity's amplitudes were abnormally higher than the THF hydrate's low frequency dispersion at 2.5MHz and 3.5MHz from the 0th min to the 300th min. Random noise was found around the lower limit of the frequency band in both experiment. Later, in the time range from the 400th min to the 570th min, the complex permittivity drastically fluctuated until the temperature broke through the 4.4°C 'platform', which indicates the dissociation process finished. Moreover, it can be observed that both the dielectric constant and loss factor of the THF solution rose as the temperature declined before the 107th min during the formation (experiment 1) and after the 570th min during the dissociation (experiment 2). These phenomena may imply mechanisms of multiphase mixture or the measuring method itself, and will be discussed in the last part of this section.

To show the temperature dependence of hydrate's permittivity, the spectrum of the THF hydrate at 2.9°C and −11.2°C fitted with the Cole-Cole model are presented in Fig 5, meanwhile, complex permittivity of THF solution at 4.4°C is taken as comparison. A steep sloop and a peak were observed in the dielectric constant and loss factor of THF hydrate in low frequency range, respectively, and the resonant frequency drifted to a lower band as the temperature decreased. For temperatures around 0°C, the index parameter α of the Cole-Cole model corresponding to THF hydrate has a relatively small value 0.018 and conductivity $\sigma = 0$S/m (both insensitivity to temperature). Early measurement of the structure II hydrates suggested that there is approximately a negative correlation between (ε_0-ε_∞) and temperature and the high frequency permittivity ε_∞ is relatively a statistical value [42]. According to the complex permittivity obtained within experiment 1 and 2, high frequency permittivity was fitted as $\varepsilon_\infty = 7$, and the proper static permittivity ε_0 as a function of absolute temperature T (in Kelvin) can be calculated as presented in equation (3) [42]. Referring to the study at lower temperature ranges [45], the relationship between relaxation time τ and the absolute temperature T

TABLE 2. Fitted cole-cole parameters of the three complex permittivity samples.

Samples	ε_∞	ε_0	τ/ sec	σ/ S/m	α
2.9°C Hydrate	7	61	4.87 e-8	0	0.018
-11.2°C Hydrate	7	63.9	8.6 e-8	0	0.018
4.4°C Soultion	5.85	67.8	1.65 e-11	3e-4	0

were concluded as equation (4).

$$\varepsilon_0 - \varepsilon_\infty = 14900/\mathrm{T} \tag{3}$$

$$\log(\tau) = -11.9 + 1265.7/\mathrm{T} \tag{4}$$

The complex permittivity of the THF solution has analogous microwave resonant properties with liquid water and its amplitude depends on volumetric ratio of THF [46], [47]. For THF solution, the Cole-Cole model was transformed to Debye type by setting α to 0. Parameters ε_0, ε_∞ and τ fitted from the experimental data matches the results in the early study fundamentally [47]. Table 2 showed the fitted Cole-Cole parameters of the three pairs of complex permittivity in Fig 5.

The fitting method in this section will be used in the calculation of component contents with mixing models in section D and E, and the fitted parameters are selected according to the recorded temperature (invariable para meters like α and σ will not be presented in the tables redundantly).

B. PERMITTIVITY DISPERSION UPON THF HYDRATE FORMATION IN POROUS MEDIA

In experiments 3 and 4, quartz sand with a diameter of 0.45mm-0.9mm and 0.18mm-0.28mm was selected as the porous matrix to study the THF hydrate formation process. Supersaturated THF solution with a 60% volumetric fraction was used as the hydrate former in these experiments. The complex permittivity measured during the formation process within the porous media is illustrated as contour maps in Figs 6 and 7 respectively. Similar to experiment 1, before the onset of the hydrate formation, the permittivity dispersion associated with the liquid THF-water solution was observed in the upper frequency range (especially apparent higher than 1GHz). By marking the abrupt change with dashed lines in the four contour maps, the characteristic of the liquid solution disappeared around the 80th min, which was earlier than in experiment 1. The most striking difference between Figs 6 and 7 appeared in the lower frequency range after the formation: in experiment 4, the slope of the permittivity was about 2 times steeper than that in experiment 3 below 100MHz. However, during the decreasing temperature period, the dispersion peak of the dielectric constant and loss factor drifted to a lower frequency in both experiment. A larger particle size weakens the dispersion peak, and it even seemed that the dispersion disappeared in Fig 6(a). Therefore, from the

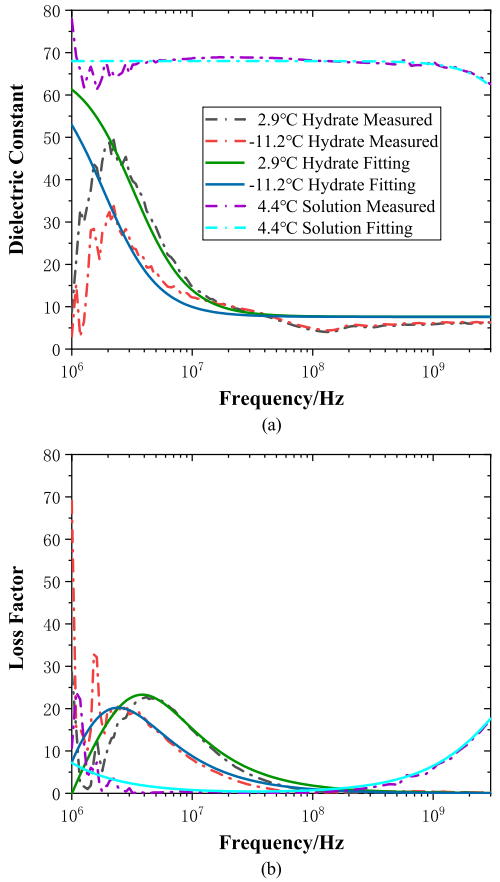

FIGURE 5. Complex permittivity spectra of THF solution and THF hydrate. Solid spectra are measured data, and dot dash spectra are fitted with Cole-Cole model: (a) dielectric constant; (b) loss factor.

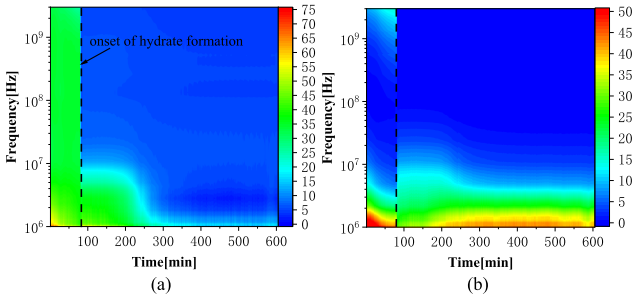

FIGURE 6. Evolution of the complex permittivity spectra as a function of time in experiment 3: (a) effect of the dielectric constant upon the THF hydrate formation process in quartz sand with a particle size of 0.45mm-0.9mm (b) effect of the loss factor upon the THF hydrate formation process in quartz sand with a particle size of 0.45mm-0.9mm.

contour maps, it can be concluded that the addition of porous media accelerates the onset of the formation. Moreover, particle size could influent the dielectric properties during and after the formation.

Four frequencies that were selected to show the permittivity and temperature as a function of time are illustrated in Figs 8 and 9. Accompanying the abrupt permittivity change around the 80th min, the formation process was initiated by a step change of temperature (red solid line) at the same time which was 30 minutes earlier than the process without

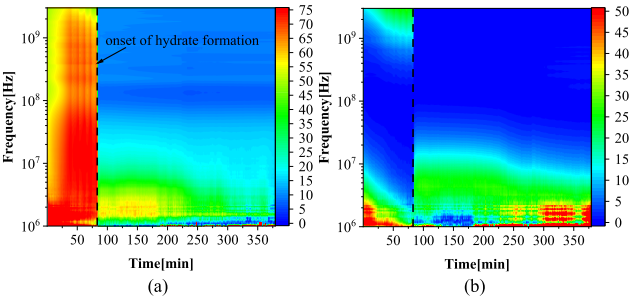

FIGURE 7. Evolution of the complex permittivity spectra as a function of time in experiment 3: (a) effect of the dielectric constant upon the THF hydrate formation process in quartz sand with a particle size of 0.18mm-0.28mm (b) effect of the loss factor upon the THF hydrate formation process in quartz sand with a particle size of 0.18mm-0.28mm.

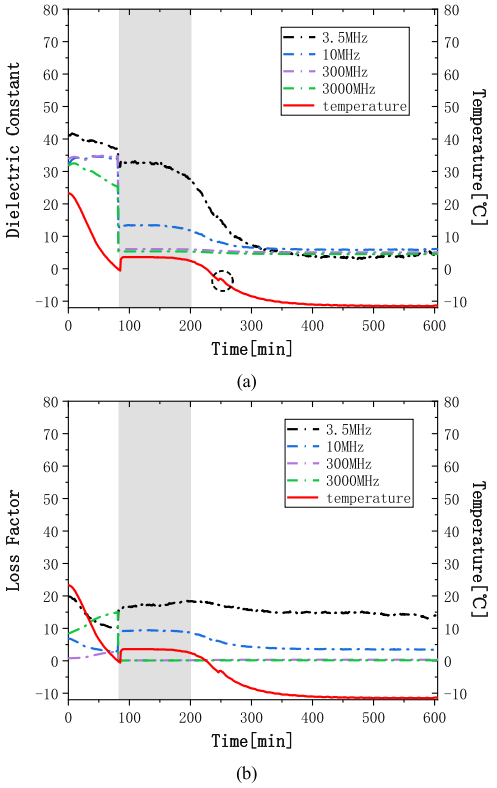

FIGURE 8. Complex permittivity at 3.5MHz, 10MHz, 300MHz, and 3GHz (dot dash line) and measured temperature (solid line) in experiment 3. Quartz sand was selected with a particle size of 0.45mm-0.9mm.

quartz sand (see data of experiment 1 in Fig 4). The dielectric constant and loss factor obtained at the four frequencies in experiments 3 and 4 before the hydrate appeared presented different changing trends. In Fig 8(a), the dielectric constant decreased at 3.5MHz and 3GHz while it remained stable at 10MHz and 300MHz, however, it changed synchronously at all frequencies in Fig 9(a); The loss factor at 3.5MHz and 10MHz decreased with time, and increased at the two higher frequencies in Fig 8(b) and Fig 9(b) in this period. The gray shaded area indicates the phase equilibrium state which signifies the time interval from the onset of the formation to the point where no solution remained inside the reactor. As soon as the formation began, the dielectric constant and loss factor

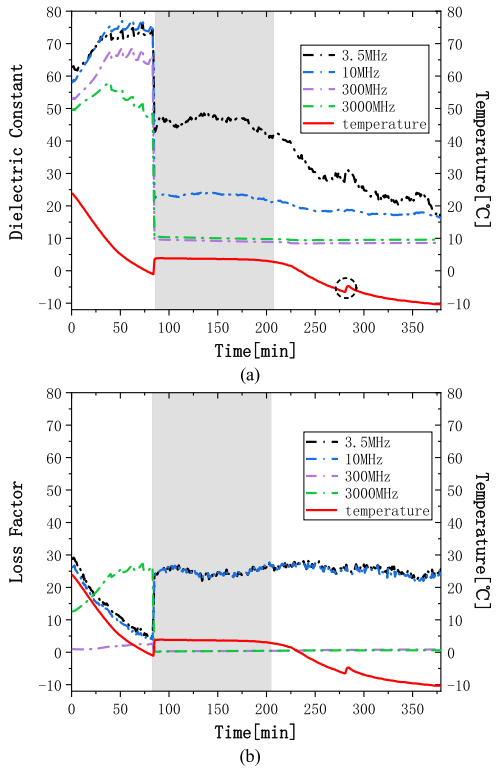

FIGURE 9. Complex permittivity at 3.5MHz, 10MHz, 300MHz, and 3GHz (dot dash line) and measured temperature (solid line) in experiment 4. Quartz sand was selected with a particle size of 0.18mm-0.28mm.

at 300MHz and 3GHz very quickly dropped to 7 and 0, respectively, and then remained steady to the end. The permittivity at 3.5MHz and 10MHz presented hydrate dispersion characteristic peaks which were analogous to experiment 1, while differences can be observed in their amplitude. In the gray shaded zone, the permittivity remained constant as the temperature stayed on the ''platform'' of phase equilibrium of the hydrate. In addition, in experiments 3 and 4, the time duration of the equilibrium state was fundamentally the same. As all the fluid converted to the hydrate, the permittivity at low frequencies dropped with the temperature. When the target temperature was achieved, all the parameters tended to be stable.

Because the detection depth of the open-ended probe is limited in several millimeters, evolution of the permittivity kept in step with the temperature measured adjacent to the probe end. With molecular polarization of water enhancement at lower temperatures, the permittivity of the THF solution increased at the higher frequency range, and at the same time, the water molecule's dispersion peak drifted to a lower frequency. Thus, changes of permittivity at 300MHz and 3GHz in Figs 8 and 9, were mainly affected by the temperature sensitivity of liquid water's dispersion before the hydrate formation started.

To show how permittivity measurements with open-ended probes can be used to monitor the hydrate formation in porous media, 10MHz was used as an example. In experiment 3, the dielectric constant and loss factor jumped to about 13 and 10 at the 80th min (formation began). As the formation continued (gray shaded area), the dielectric constant and loss factor remained t unchanged until the formation was completed. Finally, along with the decrease temperature, these two factors kept gradually dropping to about 3 (200th -400th min). Contrastively with the permittivity at 10MHz of experiment 4, the dielectric constant was 23, 22, and 16, and the loss factor was 22, 21, and 19 at the 80th min, the 200th min and the 400th min, respectively. Based on the premise that the THF solution was e prepared with the same fraction, and temperature curves showed a fundamentally analogous evaluation trend in the two experiments, only the one curve of the permittivity obtained at 10MHz could indicate differences of the two formation processes. Also, more details such as particle size and regional deposits of hydrate can be revealed from the permittivity spectrum on broad band.

Moreover, after the hydrate formation had finished, a small temperature vibration was marked with a dashed circle at the 250th min in Fig 8 and the 270th min in Fig 9. There was no simultaneous change of permittivity, so this could not be attributed to hydrate agglomerating. Inevitably there is a little water evaporation during the experiment, and as the slight temperature spring-back is located below the freezing point, it is probably due to the condensation of water vapor which is also an exothermic process.

C. PERMITTIVITY DISPERSION UPON THE THF HYDRATE DISSOCIATION IN POROUS MEIDA

In this part, the complex permittivity upon the dissociation of the THF hydrate in porous media was measured in experiments 5 and 6, and presented in Table 1. The solution proportions and porous media were the same as experiments 3 and 4, respectively. As shown in contour maps of Fig 10, with a quartz sand size of 0.45mm-0.9mm, the characteristic of the water solution dominated the permittivity spectrum after the 150th min, the dielectric constant became larger than 30 in the whole frequency range, and the loss factor rose over 1GHz. On the basis of the counter maps, it seems that the dissociation process lasted for merely 25mins in experiment 5 (between the vertical dashed lines and dotted line in Fig 10), which is a bit shorter than the pure THF hydrate, and the onset of melting was about 125mins earlier (see the spectrum in Fig 3, the dissociation began at the 250th min and was completed at the 420th min of experiment 2).

Experiment 6 was performed under the same temperature conditions, and the permittivity obtained with a quartz sand size of 0.18mm-0.28mm is shown in Fig 11. The dielectric constant began to rise at the 200th min (marked with a vertical dashed line) and the loss factor followed the same trend. The hydrate started melting at around the 200th min in experiment 6, which is much later than in experiment 5. However, it was a bit earlier than the pure THF hydrate melting process. Moreover, the loss factor presented in Fig 11(b) signified the dissociation process extremely clearly. The characteristic dispersion of the hydrate in the frequency range below 100MHz

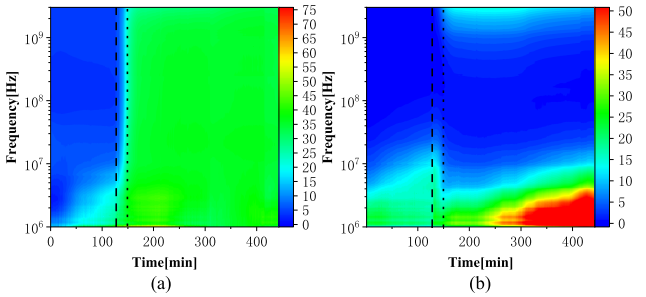

FIGURE 10. Evolution of the complex permittivity spectra as a function of time in experiment 5: (a) effect of the dielectric constant upon the THF hydrate dissociation process in quartz sand with a particle size of 0.45mm-0.9mm (b) effect of the loss factor upon the THF hydrate dissociation process in quartz sand with a particle size of 0.45mm-0.9mm.

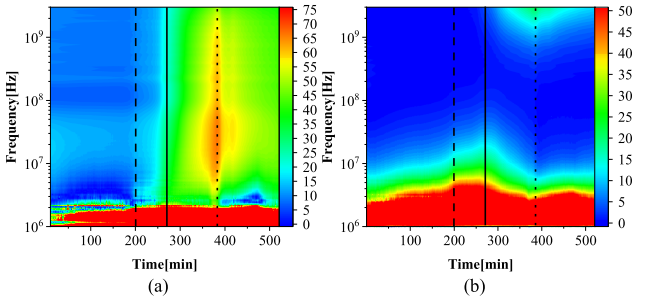

FIGURE 11. Evolution of the complex permittivity spectra as a function of time in experiment 6: (a) effect of the dielectric constant upon the THF hydrate dissociation process in quartz sand with a particle size of 0.18mm-0.28mm (b) effect of the loss factor upon the THF hydrate dissociation process in quartz sand with a particle size of 0.18mm-0.28mm.

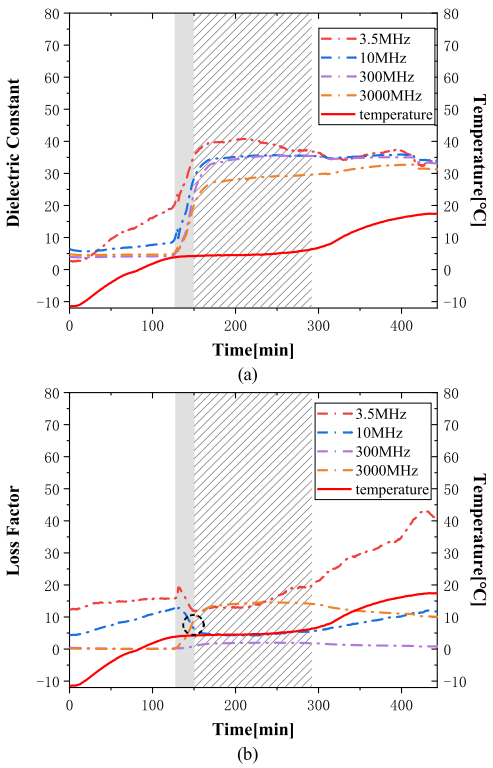

FIGURE 12. Complex permittivity at 3.5MHz, 10MHz, 300MHz, and 3GHz (dot dash line) and measured temperature (solid line) in experiment 5. Quartz sand was selected with a particle size of 0.45mm-0.9mm.

gradually drifted to a higher frequency until the 270th min (marked with a vertical solid line), and then it returned to the initial level of the experiment. A slope emerged near to the upper frequency limit after the 240th min, and the strongest amplitude was observed around the 380th min (marked with a vertical dotted line), and coincidently the low frequency "peak" had its lowest trough and then slightly rose after the 380th min until the end of the experiment.

Taking the temperature into consideration, "peaks" that reemerged after the 150th min and the 380th min in Fig 10(b) and Fig 11(b) were not induced by the polarization of water or THF molecules inside the hydrate. This is because there was no obvious increase in the dielectric constant, and the temperature (see Fig 12 and 13) was higher than the phase equilibrium point after this time. We drew w the conclusion that no THF hydrate remained inside the reactor after the 150th min in experiment 5 and the 380th min in experiment 6. In addition, particle size made the dispersion properties different during the whole experiment. The corresponding evolution of the permittivity at typical frequencies is illustrated with temperature in Figs 12 and 13.

In order to prepare the dissociation experiments, the thermotank was cooled to −12°C to make sure all the solution was completely consumed. After several hours' temperature maintenance to prevent uncontrolled hydrate melting occurring, the target temperature was set to 18°C, and the dissociation experiment began. During this procedure, a stepped temperature increase can be clearly observed in Figs 12 and 13. Initially, the temperature rose to 4.4°C at the 125th min and the 210th min in experiments 5 and 6, respectively, and then the temperature was held at 4.4°C for about 145min and 160min, respectively, which was much shorter than the dissociation process of the pure THF (320min, see Fig 4 (c) and (d)). Reviewing the result of experiment 2, the temperature broke through the 4.4°C platform with a steep rising edge at 570min (marked with a dashed circle in Fig 4), which was different from experiments 5 and 6 (the temperature more gently rose after the hydrate dissociation). Concerning the permittivity in Figs 12 and 13, more details of the phase transformation during the hydrate dissociation surrounding the probes' open-end are illustrated more definitely. Rising slopes were observed in all dielectric constant curves within the phase equilibrium platform (125min-150min in Fig 12(a) and 240min-380min in Fig 13(a)), while simultaneously the loss factor of 3.5MHz and 10MHz fell to the lowest value in the whole range at the end of the gray shaded zone in Figs 12(b) and 13(b); Moreover, there was an intersection point of the loss factor at 10MHz and 300MHz located around 145/320 min in experiments 5 and 6, which is marked with a dashed circle in Figs 12(b) and 13 (b). The permittivity change coincided with the phase equilibrium temperature in experiment 6. On the contrary, another interesting feature in the permittivity/ temperature plot was e found in experiment 5 in which the permittivity slopes did not

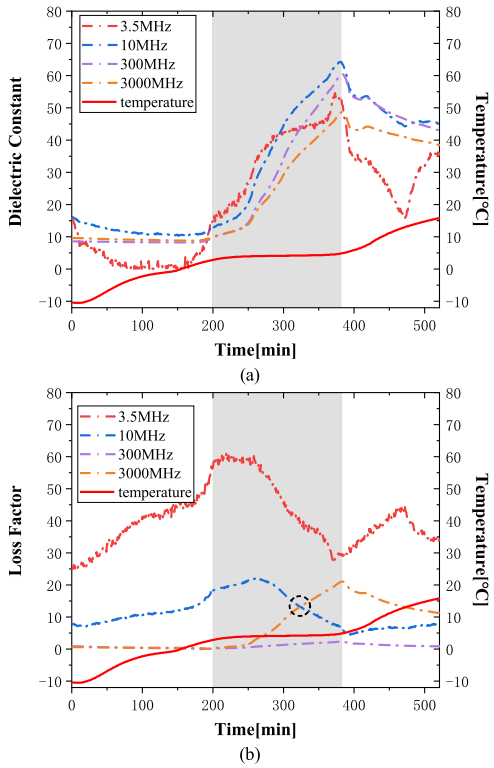

FIGURE 13. Complex permittivity at 3.5MHz, 10MHz, 300MHz, and 3GHz (dot dash line) and measured temperature (solid line) in experiment 6. Quartz sand was selected with a particle size of 0.18mm-0.28mm.

match the temperature evaluation, and as presented in Fig 12, the duration time of the phase equilibrium temperature far exceeded the permittivity change period. This indicated the hydrate melting near the probe (excess part is marked as striped shaded area in Fig 12). A similar discrepancy was also found in Fig 4, where the slopes of the permittivity occurred at the incipient stage of the phase equilibrium platform both for the pure THF hydrate and with 0.45-0.9mm quartz sand.

In this study, the permittivity information only represents the phase transition several millimeters around the probe's terminal, and hydrate melting speed detected in this small area may be significantly different from the rest of the space inside the reactor. Nevertheless, according to the equilibrium temperature duration, the total dissociation time in the two experiment was almost the same (145mins in experiment 5 and 160mins in experiment 6, only a 15mins difference). As the striped shaded area shows in Fig 12, the permittivity at all four frequencies tended to be stable following the previous gray shaded area at the phase equilibrium temperature of about 4.4°C.

D. QUANTITATIVE ESTIMATION OF THE HYDRATE PROPORTION

Estimation of the component content from the permittivity data can be robust when a proper mixing model is available [5], [7], [16], [43], [48]–[50]. In this study, CRIM (Complex Refractive Index Method) – a volume type mixing law that was feasible in previous researches on the hydrate fraction was selected to fit the measured permittivity [7].

$$\sqrt{\varepsilon^*_{\mathrm{m}}} = A\sqrt{\varepsilon^*_{sand}} + B\sqrt{\varepsilon^*_{\mathrm{solution}}} + C\sqrt{\varepsilon^*_{hydrate}} \tag{5}$$

where ε^*_m is the whole mixture's complex permittivity, and ε^*_{sand}, $\varepsilon^*_{solution}$, and $\varepsilon^*_{hydrate}$ are the complex permittivity of pure quartz sand, the THF solution, and the THF hydrate, respectively. Parameters A, B, and C are the volume fractions of pure quartz sand, the THF solution, and the THF hydrate, respectively [51]. Furthermore, under the assumption that the pore space within the matrix must be filled either with liquid or hydrate, the sum of A, B, and C should always be 100%. Quartz sand has a dielectric constant of 3.8 and a negligibly low loss factor both of which are insensitive to temperature and frequency [52]. The $\varepsilon^*_{solution}$ and $\varepsilon^*_{hydrate}$ can be calculated with the Cole-Cole model, and corresponding parameters as function of temperature were discussed above. In the following calculation, $\varepsilon^*_{solution}$ and $\varepsilon^*_{hydrate}$ were selected corresponding to temperatures from results of section 3.1. The permittivity at four time nodes are presented in Fig 14 for experiments 3 and 4. Considering that the majority of the hydrate formation took a very short time as shown in section 3.2, only the complex permittivity before and after the complete hydrate formation are presented. As shown in Fig 14 (a) and (b), the four spectra correspond to the complex permittivity at the 14th min (black dot dash line) and 46th min (red dot dash line) before hydrate formation, and the 228th min (blue dot dash line) and the 305th min (green dot dash line) after the hydrate formation of experiment 3, and the four measured spectra at the 13th min (black dot dash line) and the 45th min (red dot dash line) before the hydrate formation, and the 240th min (blue dot dash line) the 275th min (green dot dash line) after the hydrate formation of experiment 4. The measured curve became increasingly noisy with decreasing frequency, because of the sensitivity of the reflection index used for the permittivity reversion. Equation 5 was used for the hydrate fraction estimation, and the fitted permittivity is illustrated as a solid line in Fig 14.

In the permittivity spectra obtained before the hydrate formation, two dielectric dispersions occurred. The dispersion over 1GHz was due to the molecular polarization of water, and the interfacial polarization resulted in the dispersion peak below 100MHz. After the hydrate formation, only the dielectric dispersion of the THF hydrate was observed. Furthermore, as revealed from Fig 14, the dispersion properties of both the liquid solution and hydrates varied with the temperature. The THF dispersion frequency drifted to a lower band as the temperature decreased (see the 228th and 305th min in Fig 14(a) and (b), and the 240th and 275th min in Fig 14(c) and (d)). The water dispersion also moved to a lower frequency, and a slight decline was observed in the dielectric constant as the temperature decreased before the hydrate formation (see the14th and 46th min in Fig 14(a) and (b), and the 13th and 45th min in Fig 14(c) and (d)). These variation tendencies quantitatively matched experimental results

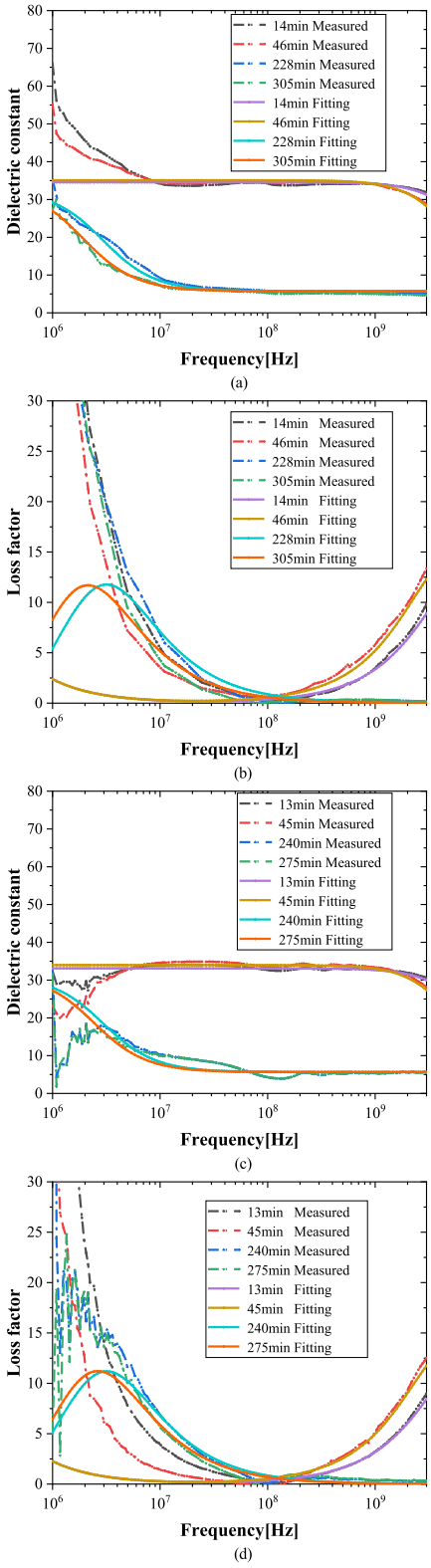

FIGURE 14. The dash dot spectra are the complex permittivity obtained with open-ended probes during experiments 3 and 4. The solid spectra were fitted to the permittivity with Cole-Cole and CRIM models. (a) The dielectric constant with a quartz sand particle size of 0.45mm-0.9mm (b) The loss factor with a quartz sand particle size of 0.45mm-0.9mm (c) The dielectric constant with a quartz sand particle size of 0.18mm-0.28mm (d) The loss factor with a quartz sand particle size of 0.18mm-0.28mm.

in previous studies, and the precise volumetric content can be determined with further calculation.

By assuming that the THF solution and the THF hydrate are dispersed in a continuous phase inside pores of the matrix (quartz sand of two particle sizes), the volumetric fraction of the THF hydrate, solution and quartz sand can be estimated using equation 5. Correspondingly, Table 3 presents the parameters A, B, and C, and the fitted data of the CRIM and Cole-Cole model were used to obtain the solid spectra in Fig 14. The Cole-Cole parameters depended on temperature, and extraordinarily, parameters of hydrate were calculated with equation 3 and 4 which were derived from the measured data. The estimated solution fractions before hydrate formation had a slight deviation from the average level – 60% given in Table 1, and this deviation was larger in experiment 3 than in experiment 4. Furthermore, a similar phenomenon was also observed after the hydrate formation in the two experiments. Additionally, parameter *A* slightly decreased after the formation process was completed, for instance, the estimated volumetric fraction of quartz sand changed from 38% at the 46th min to 37.1% at the 228th min in experiment 3.

Since the time duration of the hydrate melting process was much longer than the agglomeration, more details of component change were obtained with the fitting method mentioned above. To determine the phase transition during the dissociation process, the permittivity at six time nodes (two more extra time nodes during the dissociation process were added, the 141th and the 153th min in experiment 5 and the 309th and the 336th min in experiment 6) which are presented in Fig 15 with the corresponding temperatures. The fitted parameters are presented in Table 3. Similar to the quantitative analysis on previous formation experiments, the volumetric fraction of each component was estimated from the measured complex permittivity with the CRIM model. At the beginning, the dispersion peak of the hydrate moved to a higher band as the temperature rose (see the 18th min and the56th min of experiment 5, and the 22th min and the 130th min of experiment 6), and it was reversed when the temperature fell after the hydrate formation in Fig 14. In Fig 15 (a) and (c), the light blue and brown solid spectra were fitted before the onset of hydrate dissociation, and the dielectric constant over 100MHz was nearly flat without any perceived polarization, and hence no liquid solution is assumed to spread around the probe at this stage. Afterwards, once the temperature reached the THF hydrate's phase equilibrium state, the solid hydrate began to gradually melt. The variation of the whole measured permittivity is illustrated in Figs 12 and 13, as the temperature rose the dielectric constant increased over 100MHz, while at the same time, the amplitude of the THF hydrate's dispersion among the lower band was gradually reduced until it disappeared. Also, components fraction changes during hydrate melting were revealed by analyzing the fitted permittivity spectrum from a single measurement relying on special time nodes. It can be found in Fig 15 that the water's dispersion characteristic first began to emerge in the olive green solid spectrum over 1GHz,

TABLE 3. Parameters fitted to equation (5) during the formation process.

Experiment Number	Sand Particle Size	Temperature /°C	Time /min	A	B	C	$\varepsilon_{H\infty}$	ε_{H0}	τ_H/ sec	$\varepsilon_{S\infty}$	ε_{S0}	τ_S/ sec
Experiment 3	0.45-0.9mm	19.2	14	37.9%	0%	62.1%	None	None	None	5.85	66.67	1.15 e-11
Experiment 3	0.45-0.9mm	6.6	46	38%	0%	62%	None	None	None	5.85	67.63	1.58 e-11
Experiment 3	0.45-0.9mm	-1.1	228	37.1%	62.9%	0%	7	61.8	5.69 e-8	None	None	None
Experiment 3	0.45-0.9mm	-9	305	37.2%	62.8%	0%	7	63.44	7.84 e--8	None	None	None
Experiment 4	0.18-0.28mm	19	13	39.9%	0%	60.1%	None	None	None	5.85	66.68	1.15 e-11
Experiment 4	0.18-0.28mm	6.6	45	39.7%	0%	60.3%	None	None	None	5.85	67.63	1.58 e-11
Experiment 4	0.18-0.28mm	-1.1	240	39.1%	60.9%	0%	7	61.8	5.69 e-8	None	None	None
Experiment 4	0.18-0.28mm	-6	275	39.1%	60.9%	0%	7	62.81	6.91 e-8	None	None	None

which was obtained during the initial stage of the dissociation process. Then as the hydrate melted, the dielectric constant continued to rise in the high frequency range. The orange solid spectrum was fitted from the data obtained at a later stage of the dissociation, and the water's dispersion became more conspicuous than in the olive green spectrum. The dark blue solid spectrum had the largest numerical value of the permittivity in the high frequency range and the most prominent dispersion of water corresponded to the state where no hydrate remained. The flat dielectric constant curves at a lower frequency and at temperatures higher than 4.4°C indicated that no hydrate deposit remained inside the reactor.

More details on the experimental process were revealed from the fitted parameters of CRIM. As shown in Table 4, a larger sand particle size caused s parameter *A* to be a bit smaller corresponding to same stages in the two experiments. Before the onset of the dissociation, the hydrate fraction slightly rose with increasing temperature in both experiments. For the phase equilibrium period, first, the estimated quartz sand fraction drastically declined (from 36.9% to 22% in experiment 5 and from 39.1% to 26.5% in experiment 6), and then slightly increased, while the hydrate stock continued to be reduced and the solution accumulated during the whole equilibrium period. After the dissociation was completed, parameter *A* recovered to the level before hydrate start melting, and was even a little larger than this level. As the results showed in the previous sections, the dissociation was a relatively time-consuming process with the temperature condition stable at 4.4 °C, so the components that changed during the dissociation process cannot be estimated by only with the recorded temperature.

As discussed above, by applying the Cole-Cole and CRIM models to the permittivity, an estimation of each component's proportion can be achieved. Although there was a small deviation below 100MHz, the fitted spectra were fundamentally consistent with the experimental data. Taking the recorded temperature into consideration, a detailed analysis was made on the evolution process of the apparent hydrate's formation and dissociation.

E. ANALYSIS AND DISCUSSION

1) ERROR ANALYSIS

From results in Table 3 and 4, it can be found that the discrepancy between the estimated fractions varied among the whole experimentation process, and the relative deviation of parameter *A* (calculated by taking the prepared volumetric fraction of quartz sand 40% as standard) is smaller than 7.75% except during the phase equilibrium period in experiment 5 and 6. Inhomogeneous distribution of the measured media likely results in the nonzero deviation of the estimated volumetric fractions. Moreover, the abnormally big discrepancy could be found in parameter *A* during the dissociation period in experiment 5 and 6 (e.g. relative deviation of parameter *A* at 141th min in experiment 5 reaches 45%), because the fluid stream generated by the hydrate melting disrupt the distribution of the fluid and solid seriously. Until no hydrate left, distribution tended to be more stable and homogeneous, and the volumetric fractions estimated with CRIM came back to the values around the standard level (e.g. the relative deviation of parameter *A* decreased to 0.25% at 504th min in experiment 6).

For all the measured data exhibited above, errors were found in the spectrum blow 10MHz, which was due to the increasing uncertainty around the lower frequency limit of the open-ended coaxial method [27]. The uncertainty at low frequencies is mainly attributed to the low sensitivity in the reflection coefficient for permittivity changes at the open-end of the probe. Also, in the frequency range below 100MHz, dispersive peaks with amplitudes that are bigger than the hydrates' were observed in the period before the onset of the formation or after the dissociation was completed. As these periods were all out of the platform of the phase equilibrium state, it can be affirmed that the dispersive peaks must be related to factors other than the hydrate's dispersion.

TABLE 4. Parameters fitted to equation (5) during the dissociation process.

Experiment Number	Sand Particle Size	Temperature /°C	Time /min	A	B	C	$\varepsilon_{H\infty}$	ε_{H0}	τ_H/ sec	$\varepsilon_{S\infty}$	ε_{S0}	τ_S/ sec
Experiment 5	0.45-0.9mm	-10	18	37.1%	62.9%	0%	7	63.65	8.18 e-8	None	None	None
Experiment 5	0.45-0.9mm	-3	56	36.9%	63.1%	0%	7	62.18	6.13 e-8	None	None	None
Experiment 5	0.45-0.9mm	4.2	141	22%	53.1%	24.9%	7	60.75	4.63 e-8	5.85	67.8	1.65 e-11
Experiment 5	0.45-0.9mm	4.3	153	27%	22.4%	50.6%	7	60.73	4.62 e-8	5.85	67.8	1.65 e-11
Experiment 5	0.45-0.9mm	6.6	297	37.1%	0%	62.9%	None	None	None	5.85	67.63	1.58 e-11
Experiment 5	0.45-0.9mm	17.3	427	37.9%	0%	62.4%	None	None	None	5.85	66.81	1.22 e-11
Experiment 6	0.18-0.28mm	-10	22	39.3%	60.7%	0%	7	63.65	8.18 e-8	None	None	None
Experiment 6	0.18-0.28mm	-1.1	130	39.1%	60.9%	0%	7	61.8	5.69 e-8	None	None	None
Experiment 6	0.18-0.28mm	4.3	309	26.5%	24.4%	49.1%	7	60.73	4.62 e-8	5.85	67.8	1.65 e-11
Experiment 6	0.18-0.28mm	4.4	336	28.7%	16.7%	54.6%	7	60.71	4.6 e-8	5.85	67.8	1.65 e-11
Experiment 6	0.18-0.28mm	13	472	39.8%	0%	60.2%	None	None	None	5.85	67.1	1.39 e-11
Experiment 6	0.18-0.28mm	15	504	39.9%	0%	60.1%	None	None	None	5.85	67	1.31 e-11

The Maxwell-Wagner effect could be the most probable factor [53], [54]. Although the prepared quartz sand was well elutriated, dissolved mineral ions could increase the conductivity of the solution. On the contrary, the Maxwell-Wagner effect occurs in heterogeneous systems, however no quartz sand was installed in experiments 1 and 2, so dispersion peaks caused by interfacial polarization were not found in Figs 3 and 4.

It must be clarified that in the contour maps of Fig 3, the large amplitude below 2MHz may be due to systematic error and not the interfacial polarization. Moreover, from results in experiments 3-6 with two particle sizes, the characters of interfacial polarization varied with particle size. The experimental data and calculated spectra are presented together in Figs 14 and 15, and the fitted results almost matched the practical curves over the whole band. However, in the same time period mentioned above, serious inconformity was still found between the fitted solid spectra and measured permittivity at the lower band, and in fact, as shown in Figs 14 and 15, low frequency dispersion peaks obtained from experiments were far larger than the fitted ones. Considering the inherent inaccuracy of the open-end coaxial method around the lower frequency limit, it is assumed that there are another two factors causing these deviation: first, the scouring effect accompanying the hydrate dissociation process causes more ions to be dissolved, this discrepancy in Fig 15 is larger than in Fig 14. Second, the CRIM model is based on the weighted volumetric sum of each component's complex refractive index, so it cannot describe the interfacial dispersion caused by fundamental ion transport. To take the Maxwell-Wagner effect into account, Hanai's generalization of Bruggeman's equation [55] for two-phase mixture is used to fit the permittivity measured before the hydrate formation onset and after dissociation completed as control group (13th min in experiment 3 and 297th min in experiment 5). In this model, the volume fraction ϕ, of the dispersed phase is given as:

$$\phi = 1 - \frac{\varepsilon^*_{\text{disp}} - \varepsilon^*_m}{\varepsilon^*_{\text{disp}} - \varepsilon^*_{cont}} \left(\frac{\varepsilon^*_{cont}}{\varepsilon^*_m} \right)^{1/3} \tag{6}$$

where $\varepsilon^*_{\text{cont}}$ is the complex permittivity of the continuous phase, $\varepsilon^*_{\text{disp}}$ is the complex permittivity of the dispersed phase, and ε^*_{m} is the effective complex permittivity of the mixture. As shown in Fig 16, when THF solution and quartz sand acted as continuous phase and dispersed phase respectively, curves fitted with Hanai's formula matched the experimental data much better than with CRIM in frequency range below 100MHz. Therefore, it can be assumed that the Maxwell-Wagner effect is the likely explanation to the dispersive peaks at lower frequencies without hydrate existence. Nevertheless, in consideration of the matching effect at the whole band, a big deviation was found between the fitted parameters of Hanai's formula in Fig 16 (volume fraction of THF solution is 75.5%, and volume fraction of quartz sand is 24.5% at both 13th min and 297th min) and the reference values given in Table 1. As the interfacial polarization was not the emphasis of this study, more suitable fitting models on porous media containing hydrates will be studied and developed in our following work.

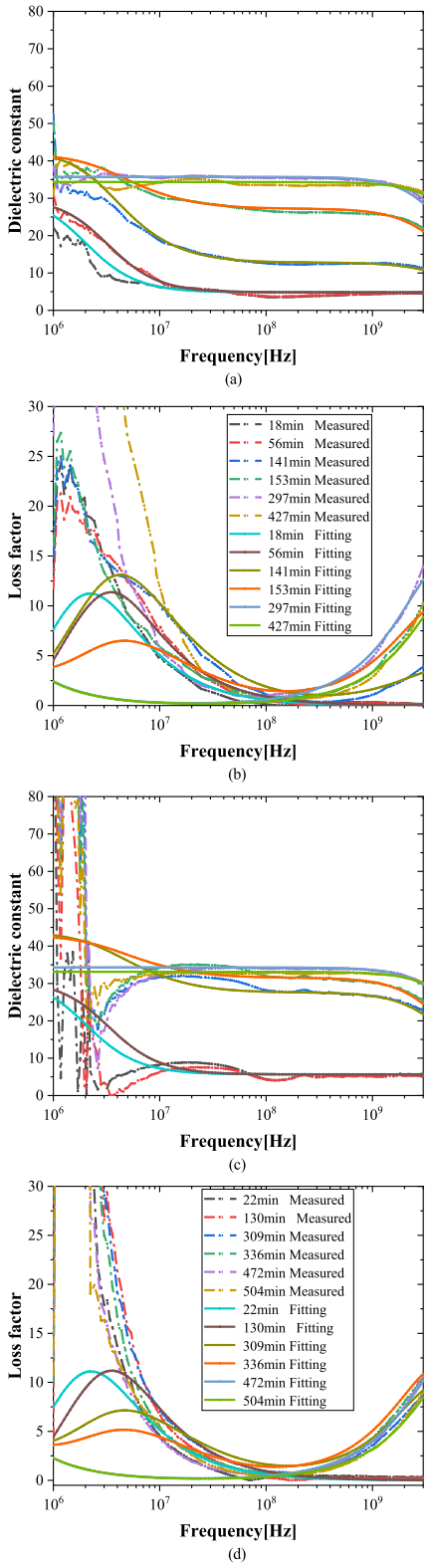

FIGURE 15. The dash dot spectra are the complex permittivity obtained with open-ended probes during experiments 5 and 6. The solid spectra were fitted to measure the permittivity with the Cole-Cole and CRIM models. (a) The dielectric constant with a quartz sand particle size of 0.45mm-0.9mm (b) The loss factor with a quartz sand particle size of 0.45mm-0.9mm (c) The dielectric constant with a quartz sand particle size of 0.18mm-0.28mm (d) The loss factor with a quartz sand particle size of 0.18mm-0.28mm.

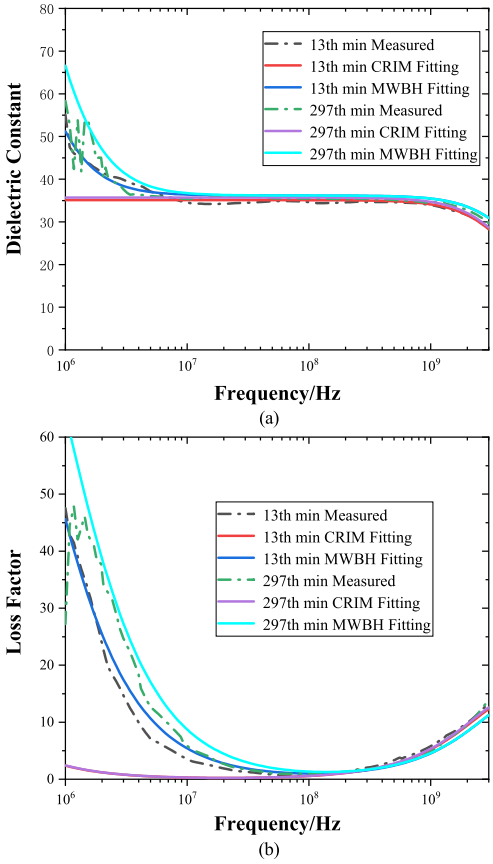

FIGURE 16. The dash dot spectra are the complex permittivity obtained with open-ended probes before formation onset and after dissociation completed in experiments 3 and 5. The solid spectra were fitted to measure the permittivity with the Hanai-Bruggeman and CRIM models. (a) The dielectric constant (b) The loss factor.

2) THE ADVANTAGES OF THE PERMITTIVITY DISPERSION MEASUREMENT

Both the temperature and permittivity can be strict indicators of the hydrate formation and dissociation [1], [7], but these two parameters did not always synchronize in this study. The most conspicuous is that during the dissociation process of the pure THF hydrate and with quartz sand of 0.45mm-0.9mm, the increasing slope of the dielectric constant indicated the accumulation of the liquid solution at the initial segment of the ''phase-equilibrium platform'', and the same for time-varying curves of the loss factor. The stable state of the equilibrium temperature was verified to indicate that phase transformation was underway in the whole space of the vessel. In other word, the phase transformation continues until the equilibrium platform breaks up. In contrast, the detection range of the open-end coaxial probe, which was stated above, approximately equals the diameter of the coaxial line, and thus the complex permittivity in only several millimeters around the probe could be precisely recorded. As a result, the deposit information of the hydrate at a particular point inside the porous media can be revealed from the dispersion properties of the complex permittivity measured with the open-end coaxial method. Practically, considering

the inhomogeneous media inside the reactor and gradient temperature on its boundary, it is possible that phase transformation process varies with position inside the reactor. Taking the results of Fig 12 as an example, the phase transformation among the permittivity measurement range was completed in the gray shaded area, and permittivity remained almost stable in the strip shaded area. As mentioned in 3.1, the permittivity of both the hydrate and the solution depends on temperature, and thus without phase transformation there would not be obvious changes in the permittivity unless the temperature changes. We can draw the conclusion that for an estimation of the hydrate in porous media at a particular point, the equilibrium temperature is necessary for phase transformation of the hydrate but it is not sufficient, while from previous analysis, the complex permittivity is definitely a coincidental indicator of the hydrate formation and dissociation.

IV. CONCLUSION

In order to develop a method to evaluate the hydrate content in porous media, the THF hydrate's formation and dissociation processes in quartz sand were monitored using permittivity measurements with the open-ended coaxial method. First, the permittivity of the pure THF hydrate was recorded as the control group, and the complex permittivity of the pure THF solution and the THF hydrate at different temperatures were tested with the Cole-Cole model and corresponding parameters varying with temperature were also calculated. Then the temperature and the complex permittivity were studied during the hydrate agglomeration and melting in quartz sand with different particle sizes. Compared with the temperature, more details were revealed both by analyzing how the permittivity varies as a function of time, and from a single permittivity spectrum at some specified time node. Results showed that the characteristic dispersion peak could be used to determine the accumulation of the hydrate, and a rising of the permittivity at low frequency indicated the formation of the hydrate, while decline at high frequency indicated a consumption of the solution liquid, and vice versa. Finally, by applying CRIM to fit the experimental data, the volumetric fraction of each component was quantitatively estimated. In conclusion, a method to monitor the existence of hydrate and evaluate its content in porous media is established with the measurement of permittivity dispersion in this study. Analysis of results presented here showed significant potential of the permittivity and its dispersion for evaluating of hydrate deposits in a porous matrix. To accurately estimate the proportion of each component in real time, further investigation still need to be carried out, and more appropriate mixing models will be established in the next research.

ACKNOWLEDGMENT

Thanks to Dr. E. C. Mignot, Shandong University, for linguistic advice.

REFERENCES

[1] E. D. Sloan, Jr., and C. A. Koh, *Clathrate Hydrates of Natural Gases*. Boca Raton, FL, USA: CRC Press, 2007.

[2] P. Englezos, "Clathrate hydrates," *Ind. Eng. Chem. Res.*, vol. 32, no. 7, pp. 1251–1274, 1993.

[3] A. V. Milkov, "Global estimates of hydrate-bound gas in marine sediments: How much is really out there?" *Earth-Sci. Rev.*, vol. 66, no. 3, pp. 183–197, 2004.

[4] M. Helgerud, J. Dvorkin, A. Nur, A. Sakai, and T. Collett, "Elastic-wave velocity in marine sediments with gas hydrates: Effective medium modeling," *Geophys. Res. Lett.*, vol. 26, no. 13, pp. 2021–2024, 1999.

[5] J. Y. Lee, J. C. Santamarina, and C. Ruppel, "Mechanical and electromagnetic properties of northern Gulf of Mexico sediments with and without THF hydrates," *Mar. Petroleum Geol.*, vol. 25, no. 9, pp. 884–895, 2008.

[6] J. Y. Lee, T. S. Yun, J. C. Santamarina, and C. Ruppel, "Observations related to tetrahydrofuran and methane hydrates for laboratory studies of hydrate-bearing sediments," *Geochem. Geophys. Geosyst.*, vol. 8, no. 6, 2007, Art. no. Q06003.

[7] J. Lee, J. C. Santamarina, and C. Ruppel, "Parametric study of the physical properties of hydrate-bearing sand, silt, and clay sediments: 1. Electromagnetic properties," *J. Geophys. Res., Solid Earth*, vol. 115, no. B11, 2010, Art. no. B11104.

[8] N. Kumar, N. B. Chowdhury, and J. G. Beltran, "A 3-in-1 approach to evaluate gas hydrate inhibitors," *Energies*, vol. 12, no. 15, p. 2921, 2019.

[9] S. Almenningen, P. Fotland, and G. Ersland, "Magnetic resonance imaging of methane hydrate formation and dissociation in sandstone with dual water saturation," *Energies*, vol. 12, no. 17, p. 3231, 2019.

[10] K. Xue, L. Yang, J. Zhao, Y. Li, Y. Song, and S. Yao, "The study of flow characteristics during the decomposition process in hydrate-bearing porous media using magnetic resonance imaging," *Energies*, vol. 12, no. 9, p. 1736, 2019.

[11] Y. Song, L. Yang, J. Zhao, W. Liu, M. Yang, Y. Li, Y. Liu, and Q. Li, "The status of natural gas hydrate research in China: A review," *Renew. Sustain. Energy Rev.*, vol. 31, no. 2, pp. 778–791, 2014.

[12] S. Pinkert, "Dilation behavior of gas-saturated methane-hydrate bearing sand," *Energies*, vol. 12, no. 15, p. 2937, 2019.

[13] K. Folgerø, K. Haukalid, J. Kocbach, and A. S. Peterson, "Combined thickness and permittivity measurement of thin layers with open-ended coaxial probes," *Sensors*, vol. 19, no. 8, p. 1765, 2019.

[14] J. Chen, K.-L. Yan, G.-J. Chen, C.-Y. Sun, B. Liu, N. Ren, D.-J. Shen, M. Niu, Y.-N. Lv, N. Li, and A. K. Sum, "Insights into the formation mechanism of hydrate plugging in pipelines," *Chem. Eng. Sci.*, vol. 122, pp. 284–290, Jan. 2015.

[15] T. Jakobsen, J. Sjöblom, and P. Ruoff, "Kinetics of gas hydrate formation in w/o-emulsions the model system trichlorofluoromethane/water/non-ionic surfactant studied by means of dielectric spectroscopy," *Colloids Surf. A, Physicochem. Eng. Aspects*, vol. 112, no. 1, pp. 73–84, 1996.

[16] T. Jakobsen and K. Folgerø, "Dielectric measurements of gas hydrate formation in water-in-oil emulsions using open-ended coaxial probes," *Meas. Sci. Technol.*, vol. 8, no. 9, p. 1006, 1997.

[17] J. H. Sa, B. R. Lee, X. Zhang, K. Folgerø, K. Haukalid, J. Kocbach, K. J. Kinnari, X. Li, K. Askvik, and A. K. Sum, "Hydrate management in deadlegs: Detection of hydrate deposition using permittivity probe," *Energy Fuel*, vol. 32, no. 2, pp. 1693–1702, 2018.

[18] K. Haukalid, K. Folgerø, T. Barth, and S. L. Fjermestad, "Hydrate formation in water-in-crude oil emulsions studied by broad-band permittivity measurements," *Energy Fuel*, vol. 31, no. 4, pp. 3793–3803, 2017.

[19] H. Masayuki, N. Yukio, Y. Norimasa, and E. Toshiro, "Basic research on the mechanical behavior of methane hydrate-sediments mixture," *Soils Found.*, vol. 45, no. 1, pp. 75–85, 2005.

[20] A. Masui, K. Miyazaki, H. Haneda, Y. Ogata, and K. Aoki, "Mechanical characteristics of natural and artificial gas hydrate bearing sediments," in *Proc. 6th Int. Conf. Gas Hydrates*, 2008, pp. 6–10.

[21] T. S. Yun, J. C. Santamarina, and C. Ruppel, "Mechanical properties of sand, silt, and clay containing tetrahydrofuran hydrate," *J. Geophys. Res., Solid Earth*, vol. 112, no. B4, 2007, Art. no. B04106.

[22] Y.-H. Li, Y.-C. Song, F. Yu, W.-G. Liu, and J.-F. Zhao, "Experimental study on mechanical properties of gas hydrate-bearing sediments using kaolin clay," *China Ocean Eng.*, vol. 25, no. 1, p. 113, 2011.

[23] M. Hyodo, Y. Li, J. Yoneda, Y. Nakata, N. Yoshimoto, A. Nishimura, and Y. Song, "Mechanical behavior of gas-saturated methane hydrate-bearing sediments," *J. Geophys. Res., Solid Earth*, vol. 118, no. 10, pp. 5185–5194, 2013.

[24] J.-Y. Lee, "Hydrate-bearing sediments: Formation and geophysical properties," Ph.D. dissertation, Georgia Inst. Technol., Atlanta, GA, USA, 2007.

[25] U. Majumdar, A. E. Cook, M. Scharenberg, A. Burchwell, S. Ismail, M. Frye, and W. Shedd, "Semi-quantitative gas hydrate assessment from petroleum industry well logs in the northern Gulf of Mexico," *Mar. Petroleum Geol.*, vol. 85, pp. 233–241, Aug. 2017.
[26] Y. Sun, D. Goldberg, T. Collett, and R. Hunter, "High-resolution well-log derived dielectric properties of gas-hydrate-bearing sediments, Mount Elbert Gas Hydrate Stratigraphic Test Well, Alaska North Slope," *Mar. Petroleum Geol.*, vol. 28, no. 2, pp. 450–459, 2011.
[27] K. Haukalid and K. J. Folgerø, "Broad-band permittivity measurements of formation of gas hydrate layers using open-ended coaxial probes," *Energy Fuel*, vol. 30, no. 9, pp. 7196–7205, 2016.
[28] J. Santamarina, F. Francisca, T. Yun, J. Lee, A. Martin, and C. Ruppel, "Mechanical, thermal, and electrical properties of hydrate-bearing sediments," in *Proc. AAPG Hedberg Conf. Gas Hydrates: Energy Resource Potential Assoc. Geol. Hazards.*, Vancouver, BC, Canada, 2004, pp. 1–4.
[29] R. Pérez-Aparicio, D. Cottinet, C. Crauste-Thibierge, L. Vanel, P. Sotta, J.-Y. Delannoy, D. R. Long, and S. Ciliberto, "Dielectric spectroscopy of a stretched polymer glass: heterogeneous dynamics and plasticity," *Macromolecules*, vol. 49, no. 10, pp. 3889–3898, 2016.
[30] S. A. Komarov, A. S. Komarov, D. G. Barber, M. J. L. Lemes, and S. Rysgaard, "Open-ended coaxial probe technique for dielectric spectroscopy of artificially grown sea ice," *IEEE Trans. Geosci. Remote Sens.*, vol. 54, no. 8, pp. 4941–4951, Aug. 2016.
[31] M. V. Traffano-Schiffo, M. Castro-Giraldez, V. Herrero, R. J. Colom, and P. J. Fito, "Development of a non-destructive detection system of deep pectoral myopathy in poultry by dielectric spectroscopy," *J. Food Eng.*, vol. 237, pp. 137–145, Nov. 2018.
[32] G. G. B. Nielsen, A. Kjær, B. Klösgen, P. L. Hansen, A. C. Simonsen, and B. Jørgensen, "Dielectric spectroscopy for evaluating dry matter content of potato tubers," *J. Food Eng.*, vol. 189, pp. 9–16, Nov. 2016.
[33] A. K. Jha and M. J. Akhtar, "A generalized rectangular cavity approach for determination of complex permittivity of materials," *IEEE Trans. Instrum. Meas.*, vol. 63, no. 11, pp. 2632–2641, Nov. 2014.
[34] K. Takeya, R. Takahashi, T. Fukui, S. R. Tripathi, and K. Kawase, "Terahertz characterization of propane hydrate," *Jpn. J. Appl. Phys.*, vol. 58, no. 3, 2019, Art. no. 032003.
[35] D. Kawakami and H. Tabata, "THz-TDS measurements of hydration state of bio related materials and data analysis by machine learning," in *Proc. 43rd Int. Conf. Infr., Millim., THz. Waves (IRMMW-THz)*, Sep. 2018, p. 1.
[36] M. Tyagi and S. S. N. Murthy, "Dielectric relaxation in ice and ice clathrates and its connection to the low-temperature phase transition induced by alkali hydroxides as dopants," *J. Phys. Chem. A*, vol. 106, no. 20, pp. 5072–5080, 2002.
[37] W. S. Brey, Jr., and H. P. Williams, "Dielectric properties of ice and water clathrates," *J. Phys. Chem.*, vol. 72, no. 1, pp. 49–52, 1968.
[38] D. Davidson and J. Ripmeester, "Clathrate ices—Recent results," *J. Glaciol.*, vol. 21, no. 85, pp. 33–49, 1978.
[39] S. Evans, "Dielectric properties of ice and snow—A review," *J. Glaciol.*, vol. 5, no. 42, pp. 773–792, 1965.
[40] A. K. Jonscher, "The 'universal' dielectric response," in *Proc. Conf. Elect. Insul. Dielectr. Phenomena*, vol. 267, 2002, pp. 673–679.
[41] F. Franks, *Water A Comprehensive Treatise: Aqueous Solutions of Amphiphiles and Macromolecules*, vol. 4. New York, NY, USA: Plenum Press, 1975.
[42] S. R. Gough, R. E. Hawkins, B. Morris, and D. W. Davidson, "Dielectric properties of some clathrate hydrates of structure II," *Can. J. Chem.*, vol. 77, no. 25, pp. 2969–2976, 1973.
[43] K. Asami, "Characterization of heterogeneous systems by dielectric spectroscopy," *Prog. Polym. Sci.*, vol. 27, no. 8, pp. 1617–1659, 2002.
[44] B. Morris and D. W. Davidson, "A clathrate hydrate of cyclobutanone: Dielectric relaxation of the host and guest molecules," *Can. J. Chem.*, vol. 49, no. 49, pp. 1243–1251, 1971.
[45] R. E. Hawkins and D. W. Davidson, "Dielectric relaxation in the clathrate hydrates of some cyclic ethers," *J. Phys. Chem.*, vol. 70, no. 6, pp. 1889–1894, 1966.
[46] F. E. Critchfield, J. A. Gibson Jr, and J. L. Hall, "Dielectric constant and refractive index from 20 to 35° and density at 25° for the system tetrahydrofuran–water," *J. Amer. Chem. Soc.*, vol. 75, no. 23, pp. 6044–6045, 1953.
[47] A. C. Kumbharkhane, S. N. Helambe, M. P. Lokhande, S. Doraiswamy, and S. C. Mehrotra, "Structural study of aqueous solutions of tetrahydrofuran and acetone mixtures using dielectric relaxation technique," *Pramana*, vol. 46, no. 2, pp. 91–98, 1996.
[48] K. Haukalid and K. Folgerø, "Dielectric mixture models for hydrate formation and agglomeration," in *Proc. 12th Int. Conf. Electromagn. Wave Interact. Water Moist Substances (ISEMA)*, Jun. 2018, pp. 1–9.
[49] A. H. Sihvola and J. A. Kong, "Effective permittivity of dielectric mixtures," *IEEE Trans. Geosci. Remote Sens.*, vol. GRS-26, no. 4, pp. 420–429, Jul. 1988.
[50] Y. Chen and D. Or, "Geometrical factors and interfacial processes affecting complex dielectric permittivity of partially saturated porous media," *Water Resour. Res.*, vol. 42, no. 6, 2006, Art. no. W06423.
[51] V. L. Mironov, M. C. Dobson, V. H. Kaupp, S. A. Komarov, and V. N. Kleshchenko, "Generalized refractive mixing dielectric model for moist soils," *IEEE Trans. Geosci. Remote Sens.*, vol. 42, no. 4, pp. 773–785, Apr. 2004.
[52] C. Matzler, "Microwave permittivity of dry sand," *IEEE Trans. Geosci. Remote Sens.*, vol. 36, no. 1, pp. 317–319, Jan. 1998.
[53] O. A. L. de Lima and M. M. Sharma, "A generalized Maxwell-Wagner theory for membrane polarization in shaly sands," *Geophysics*, vol. 57, no. 3, pp. 431–440, 1992.
[54] Y. Chen and D. Or, "Effects of Maxwell-Wagner polarization on soil complex dielectric permittivity under variable temperature and electrical conductivity," *Water Resour. Res.*, vol. 42, no. 6, 2006, Art. no. W06424.
[55] T. Hanai, "Theory of the dielectric dispersion due to the interfacial polarization and its application to emulsions," *Kolloid-Zeitschrift*, vol. 171, no. 1, pp. 23–31, 1960.

BIN WANG received the B.S. degree in applied physics from Qingdao University, in 2010, and the Ph.D. degree in radio physics from Shandong University, China, in 2015.

From 2015 to 2017, he was a Lecturer with the China University of Petroleum (East China). Since 2018, he has been an Associate Professor. His research interests include detection technology and automatic device, permittivity measurement, dielectric logging method, measurement of gas hydrate, and numerical simulation method of electromagnetic.

ZHONGHAO ZHANG received the B.S. degree in building electrical and intelligent engineering from the School of Information and Electrical Engineering, Shandong Jianzhu University, in 2017. He is currently pursuing the M.S. degree with the College of Control Science and Engineering, China University of Petroleum (East China), Qingdao, China.

From 2017 to 2019, he was a graduate student with the China University of Petroleum (East China). His research interests include detection technology and automatic device.

LANCHANG XING (M'17) received the B.S. degree in automation and the M.S. degree in control science and engineering from the China University of Petroleum (East China), in 2005 and 2008, respectively, and the Ph.D. degree in process system engineering from Cranfield University, U.K., in 2012.

From 2012 to 2015, he was a Lecturer with the China University of Petroleum (East China). Since 2016, he has been an Associate Professor. His research interests include detection technology and automatic device, computer measurement and control systems, measurement of gas hydrate and multiphase flow, and multiphysical field coupling numerical simulation method.